Accepted Manuscript

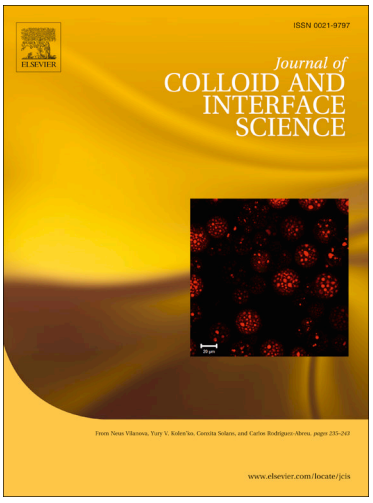

Tunable Fluorescence Quenching near the Graphene-Aqueous Interface

Aaron W. Chen, Alejandro L. Briseno, Maria M. Santore

PII: S0021-9797(17)30786-5
DOI: http://dx.doi.org/10.1016/j.jcis.2017.07.019
Reference: YJCIS 22548

To appear in: *Journal of Colloid and Interface Science*

Received Date: 15 May 2017
Revised Date: 4 July 2017
Accepted Date: 5 July 2017

Please cite this article as: A.W. Chen, A.L. Briseno, M.M. Santore, Tunable Fluorescence Quenching near the Graphene-Aqueous Interface, *Journal of Colloid and Interface Science* (2017), doi: http://dx.doi.org/10.1016/j.jcis.2017.07.019

This is a PDF file of an unedited manuscript that has been accepted for publication. As a service to our customers we are providing this early version of the manuscript. The manuscript will undergo copyediting, typesetting, and review of the resulting proof before it is published in its final form. Please note that during the production process errors may be discovered which could affect the content, and all legal disclaimers that apply to the journal pertain.

ACCEPTED MANUSCRIPT

Tunable Fluorescence Quenching near the Graphene-Aqueous Interface

Aaron W. Chen, Alejandro L. Briseno, and Maria M. Santore*

Department of Polymer Science and Engineering
University of Massachusetts
Amherst, MA 01003

Abstract

With increased interest in graphene-based sensors for biomolecules and other targets, we investigated the impact of ionic strength on the steady-state emissions from fluorescein labels on proteins adsorbing on pristine CVD (chemical vapor deposited)-graphene on a silica support. Using the model system of fluorescein-tagged fibrinogen we demonstrated that, for fluorescein tags on adsorbed fibrinogen, emission intensity was very sensitive to the salt concentration. This behavior was not seen for fluorescein-tagged fibrinogen in solution. We demonstrated that fluorescein "quenching" in this system was a result of fluorescein's pH sensitivity: with changes in salt concentration, near-surface fluorescein experiences either the neutral bulk pH or, with a negatively charged surface, an acidic environment. The findings carry the important implication that the aqueous environment near silica-supported graphene is substantially acidic as a result of near surface negative charge. This further implies, because of the purity of the graphene in this study and its lack of oxidation, that negative charge arises from ion adsorption and/or from the underlying silica support, which may be hydrated and present dissociated surface silanols. That is, the electrostatic potential from silica beneath the graphene may pass through the graphene, much as van der Waals interactions have been proven to do. Results were semi-quantitatively consistent with calculations that employed a Guoy Chapman model of the interface and the established pKa of the fluorescein. While these findings were obtained with adsorbed proteins, similar fluorescence quenching would be expected for any fluorescein-tagged species in the vicinity of silica-supported graphene. Thus, because of the negative charge at the aqueous graphene interface, ionic strength can be exploited as means of creating a molecular ruler of fluorescein emissions, and the emissions can be assessed within different distances, corresponding to the Debye length, from the graphene interface.

Keywords: graphene, protein adsorption, fluorescence quenching, biosensor

ACCEPTED MANUSCRIPT

ACCEPTED MANUSCRIPT

Introduction

The potential for graphene-based materials to improve sensing technology stems from their combined electronic and optical properties. Highly-conjugated single atomic sheets can facilitate flexible circuitry but can also interact, on active sensor pads, in unique ways with target species, including fluorescent labels on those targets.[1-6] The latter has motivated the incorporation of graphitic layers (graphene, but also graphene oxide (GO) and reduced graphene oxide (rGO)) in sensors for a variety of species from ions to proteins, DNA, and cells.[7-12] In many of these sensing applications, the steady state intensity emitted from flouorophores approaching graphitic layers is measurably reduced, sometimes almost completely.[13-15] The community has broadly referred to this as "quenching."[2, 6, 11-13, 15] Formally, quenching via resonance energy transfer requires interaction of the dipoles of fluorophores and graphene.[16-18] Electron charge transfer is a second mechanism by which quenching can occur, but is very short range.[19] Reabsorption of emitted photons can separately reduce the measured steady state emissions. Indeed graphene is an excellent absorber of visible light.[20]

Regardless of the exact mechanism, which is not always quantified, the decreased steady-state emission intensity from fluorophores near graphitic materials, even at distances of tens of nanometers, is established and aligned with sensing applications.[2, 6, 11-13, 15, 21] The greater effective quenching of graphene, compared with graphene oxide,[14] is consistent with the expected reduction in quenching caused by flaws, oxidation, and edges. Nonetheless these flaws and oxidation in graphene oxide are well tolerated in sensing applications. Additionally, the steady state emission intensity from flouorophores within

ACCEPTED MANUSCRIPT

tens of nanometers from graphene has been proposed as a method to characterize the layer numbers and extents of oxidation in supported graphene, GO, and rGO layers.[13, 19, 22] A seminal work comparing these materials in films and in suspensions, and evaluating several fluorophores has been accepted by many as evidence that graphitic materials are "general quenchers."[12, 23] Modeling explains that (pristine) graphene quenching of fluorophores via resonance energy transfer acts at distances of up to 30 nm.[24-26]

The long-range quenching behavior of graphene could be exploited in many settings; however, it would also be generally useful to tune the interactive range between graphene and fluorophores, for instance to 1-2 nm or 4-5 nm, potentially commensurate with the size of target molecules that bear fluorescent labels. This goal, pursued here in the context of supported large-area CVD (chemical vapor deposited) graphene for use in biosensors, requires an understanding of the near-graphene aqueous environment and how it can be manipulated it to influence interactions with fluorophores.

While the work function of graphene can be altered through the choice of support and overlayers[27-29] and, while van der Waals interactions can be manipulated through the number of graphene layers and choice of substrate,[30-32] electrostatic interactions are particularly important in aqueous systems and amenable to manipulation. Indeed, we recently demonstrated the presence of interfacial negative charge near silica-supported large area CVD graphene, resulting in colloidal-scale repulsions.[33] This negative interfacial charge should also be evident in emissions from appropriately-positioned pH- sensitive fluorophores, such as fluorescein. Notably fluorescein is an important label used in both

ACCEPTED MANUSCRIPT

biomolecular graphene sensors[15, 34-37] and in the seminal fluorescence quenching microscopy work.[13]

In this paper we demonstrate how ionic strength can be used to tune fluorescence from fluorescein-tagged fibrinogen (FITC-fibrinogen) adsorbed to silica-supported CVD graphene. The investigation focuses on 'large area' CVD graphene, estimated at 2-3 layers thick based on its Raman spectrum which also evidences a pristine sp2 character with no detectible sp3 bonds. Calculations of the near-surface equilibrium between nonfluorescent anion and fluorescent dianion forms of fluorescein are compared with the fluorescence data and demonstrate how fluorescence provides an interfacial ruler on the length scale of the Debye length (potentially from about 0.5 to 8 nm). The results also demonstrate that quenching is screened by ions but is substantial in deionized water. The results imply that, despite graphene's substantially hydrophobic character (evidenced by contact angle), the aqueous character of silica-supported graphene is charged, possibly as a result of the silica itself. Taken together with prior findings that silica-supported CVD graphene repels silica microsphere in an ionic strength-dependent manner, the current study further supports the interpretation of negative charge near silica-supported graphene.

ACCEPTED MANUSCRIPT

ACCEPTED MANUSCRIPT

Experimental Details

The silica-supported CVD graphene in this work is identical to that in our study of colloidal interactions.[33] Briefly, graphene was formed from a methane precursor on copper by chemical vapor deposition at 1000°C. Polymethylmethacrylate (PMMA) was then spincast on top of the graphene, and the copper removed by etching in iron chloride. The solution was twice replaced with DI (deionized) water to remove etchant. The film was then transferred, graphene-side down, onto a microscope slide that had been etched overnight in sulfuric acid and rinsed with copious amounts of DI water. The acid-etched surface of the slide comprises a layer of silica. The PMMA was then removed by rinsing with acetone and any residue was further removed by annealing at 240 °C for 1 hour in a nitrogen stream. The complete removal of PMMA was evidenced by XPS (x-ray photoelectron spectroscopy), with data presented previously.[33] Additional characterization by Raman spectroscopy further confirmed the lack of sp3 carbons and a graphene surface having between 2 and 3 layers, in the supporting information of that prior reference. Additional characterization by AFM (atomic force microscopy) and contact angle was reported in our prior studies. Notably, an advancing contact angle of 76.8 °± 4.2° was measured for the supported graphene, distinguishing it from bare silica. The same silica substrate without the graphene was employed as a control surface.

Protein adsorption and rinse solutions were pH 7.4 phosphate buffer (0.008M, Na_2HPO_4 plus 0.002M KH_2PO_4), which had an ionic strength of 0.026M and a Debye length, κ^{-1} = 2 nm. This main buffer was diluted with DI water as needed to produce a series of pH 7.4

ACCEPTED MANUSCRIPT

buffered solutions of lower ionic strength and greater Debye length, up to 8 nm. Higher ionic strength buffer with κ^{-1} = 0.74 and 1 nm was produced by adding 0.15 M NaCl to the initial buffer.

Bovine serum fibrinogen, fraction I type I-S, was purchased from Sigma Aldrich (CAS 9001-32-5). It, was tagged with fluorescein isothiocyanate isomer I from Aldrich (CA 3326-32-7) in pH 9 carbonate buffer (0.046 M $NaHCO_3$ plus 0.004 M Na_2CO_3) following established procedures.[38] To remove excess free label from the fibrinogen solution, it was eluted through a Bio-Gel P-6 column (Bio-Rad Laboratories) in pH 7.4 buffer. This process also returned the protein to pH 7.4 buffer. The density of fluorescein labeling was quantified by absorbance at 278 and 493 ± 2 nm for the protein and dye respectively, in a Shimadzu UV-VIS spectrofluorometer. Labeling densities were usually in the range 3-7 per protein molecule, in a given batch. A highly densely labeled solution of 10 fluoresceins/fibrinogen was employed in additional experiments to reproduce results done with lighter labeling, to establish that labeling density did not influence results. We previously determined[39, 40] that the diffusion coefficient of fibrinogen,[41, 42] 2.1 x 10-7 cm^2/s is not altered by fluorescent labeling. Also worth noting, fibrinogen carries a net negative charge, having a point of zero net charge at pH 5.9 and, at pH 7.4, a zeta potential that varies from -7 to -20 mV as the concentration of NaCl is varied from 0.001 to 0.15 M.[43]

Fibrinogen adsorption and the fluorescence from adsorbed FITC-fibrinogen layers was studied in a custom total internal reflectance fluorescence (TIRF) chamber configured in a modified sample compartment of a Spex II Fluorolog. The test surface comprised one wall

ACCEPTED MANUSCRIPT

of a laminar slit flow chamber and light was guided and totally internally reflected in the test substrate using a prism. Fluorescence was monitored in real time with excitation at 488 nm and emission at 520 nm. In studies of solution-phase fluorescence, a standard cuvette was employed, using the same excitation and emission wavelengths.

Near-Brewster reflectometry was employed in a control experiment to track fibrinogen adsorption on silica. Near-Brewster reflectometry comprises by a second, mass-sensitive method for comparison with TIRF. Near-Brewster reflectometry, which reports adsorbed mass by sensing the near-surface refractive index, has been described in detail previously.[44] The same flow chamber was employed in the Brewster experiment that was used in the TIRF studies.

ACCEPTED MANUSCRIPT

ACCEPTED MANUSCRIPT

Results

General features of Adsorption. Figure 1 shows nearly identical adsorption kinetics, coverages, and substantial retention of FITC-fibrinogen on graphene and on the silica control surface. Adsorption was conducted in flowing pH 7.4 phosphate buffer, having an ionic strength of 0.026M and a Debye length of κ^{-1}= 2 nm. The fluorescence signal was normalized on the baseline value, which accounts for scattering and is proportional to the lamp intensity. The buffer was chosen as the "main" buffer for the study as it contains the buffering ion content of phosphate buffered saline but lacks the added NaCl. The supported graphene was fully characterized, and contains between 2 and 3 layers.[33] The FITC-fibrinogen layers established on the two surfaces are similar, stable, and form the basis for the study of fluorophore quenching in proximity to graphene.

We note, as an aside, that the adsorption of negatively-charged proteins to negatively-charged surfaces is not unusual and that fibrinogen has substantial established adsorption on silica.[45-47] The reproducibly rapid initial kinetics on both surfaces is consistent with transport-limited behavior.[39, 40] Factors contributing to the ultimate coverage generally include the conformation[46, 47] of the protein and can be sensitive to experimental conditions.[39, 40] Detailed study of fibrinogen adsorption kinetics and the ultimate coverage on graphene is outside the current scope. Fibrinogen is employed here as model test protein. However, worth noting, all adsorption was conducted at the same conditions in this study to facilitate a comparison between the supported graphene substrate and the bare silica, in terms of the emissions from the fluorescein labels.

ACCEPTED MANUSCRIPT

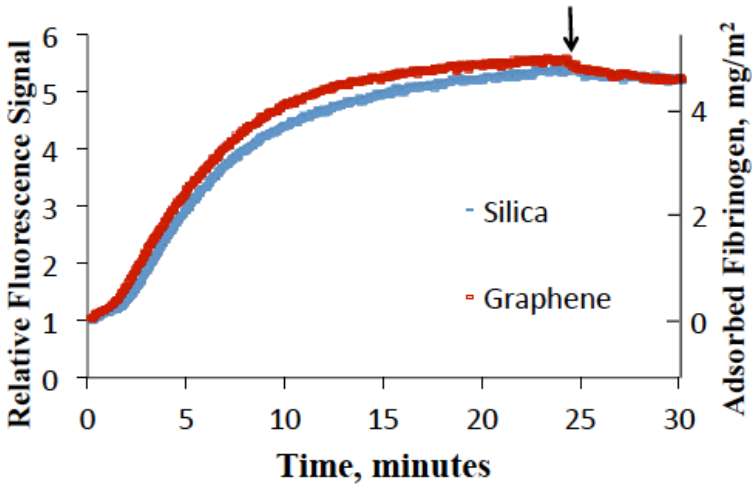

Figure 1. TIRF signal during adsorption of fibrinogen on silica-supported graphene and on silica (control) from a pH 7.4 buffered bulk solution having 25ppm fibrinogen, and a wall shear rate of 5 s^{-1}. Adsorption starts at time zero and buffer replaces flowing protein solution at the arrow.

Eliminating the hypotheses of photobleaching and mass loss. A gradual decay reduces the long time fluorescence on both surfaces in Figure 2, and must be addressed before quenching is systematically imposed. To determine any role of photobleaching in causing the decays, Figure 2A compares two TIRF runs tracking adsorption of FITC-fibrinogen on silica: one with continuous illumination and a second in which the lamp shutter is closed, keeping the surface dark during most of the ~2 hour period in which buffer flows. Then the lamp shutter is opened. The return of the signal to same fluorescence level observed with continuous illumination rules out photobleaching as the cause of the signal decay.

ACCEPTED MANUSCRIPT

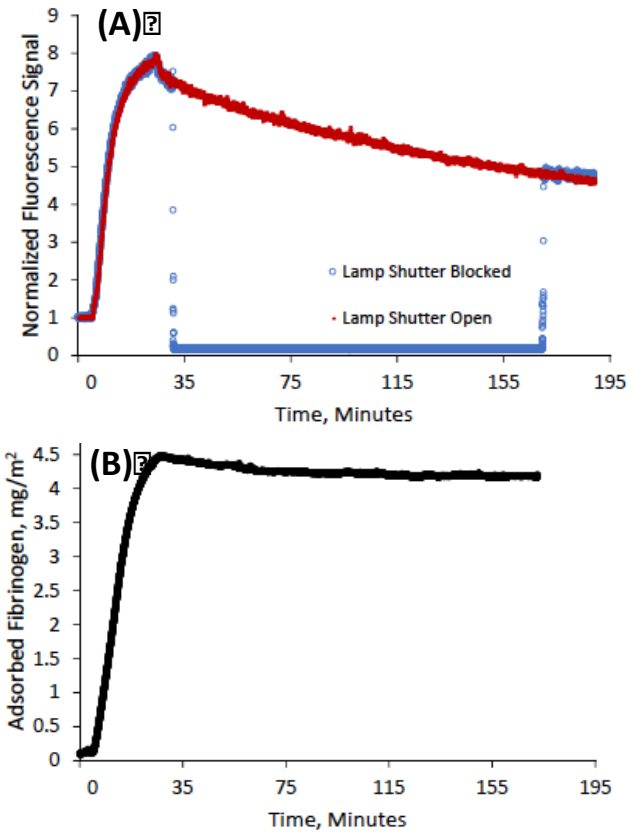

Figure 2. (A) Adsoprtion runs on silica, comparing continuous illumination to the case where the shutter was closed and later opened. (B) Near Brewster reflectometry study of adsorbed Fibrinogne on silca.

In Figure 2B, adsorption of FITC-fibrinogen on silica is repeated, with the signal measured by near-Brewster reflectivity, proportional to interfacial mass, instead of TIRF which depends on the fluorescent label number and the fluorescence per fluorophore. (Indeed reflectometry, which has an optical calibration,[44] was employed to calibrate the interfacial mass in Figure 1.) Figure 2B exhibits substantially less long-time signal loss, which would correspond to a loss of interfacial protein, during the buffer flow compared with Figure 1, suggesting that the fluorescence decay in Figure 1 was primarily due to a change in the fluorescence efficiency with time. Only a small amount of protein desorption, contributed to the signal decay.

ACCEPTED MANUSCRIPT

The best explanation of the long time signal decay in Figure 1 is slow protein reconformation over a period of hours in flowing buffer. A small amount of protein desorption, corresponding to the most weakly bound population, is a secondary effect. While slow protein relaxations are secondary to the main message of this paper, they produce a long-time signal decay that will be separated from the impact of ionic strength, which will be imposed on shorter timescales.

Reversible Fluorescence Switching. Figure 3 shows the reversible fluorescence changes that result from variations in the ionic strength of the buffer flowing over adsorbed FITC-fibrinogen layers. In Figure 3A for a supported graphene surface and Figure 3B for bare silica, the FITC-fibrinogen adsorption itself is conducted in buffer having a Debye length of 2 nm, which is reinjected after completion of the adsorption step, similar to Figure 1. A series of other pH 7.4 buffers are then introduced and, after a stable signal is recorded with each, the original κ^{-1} =2 nm buffer is rejected before moving on to the next buffer with its new ionic strength. The lower ionic strength buffers (with κ^{-1} >2) are introduced early in the series. The higher ionic strength buffers are introduced later because these partially desorb the FITC-fibrinogen from the silica. Evident in both runs of Figure 3 is an underlying fluorescence decay during flowing buffer(s) that resembles that in Figure 2A, and is not attributable to photobleaching or protein removal.

ACCEPTED MANUSCRIPT

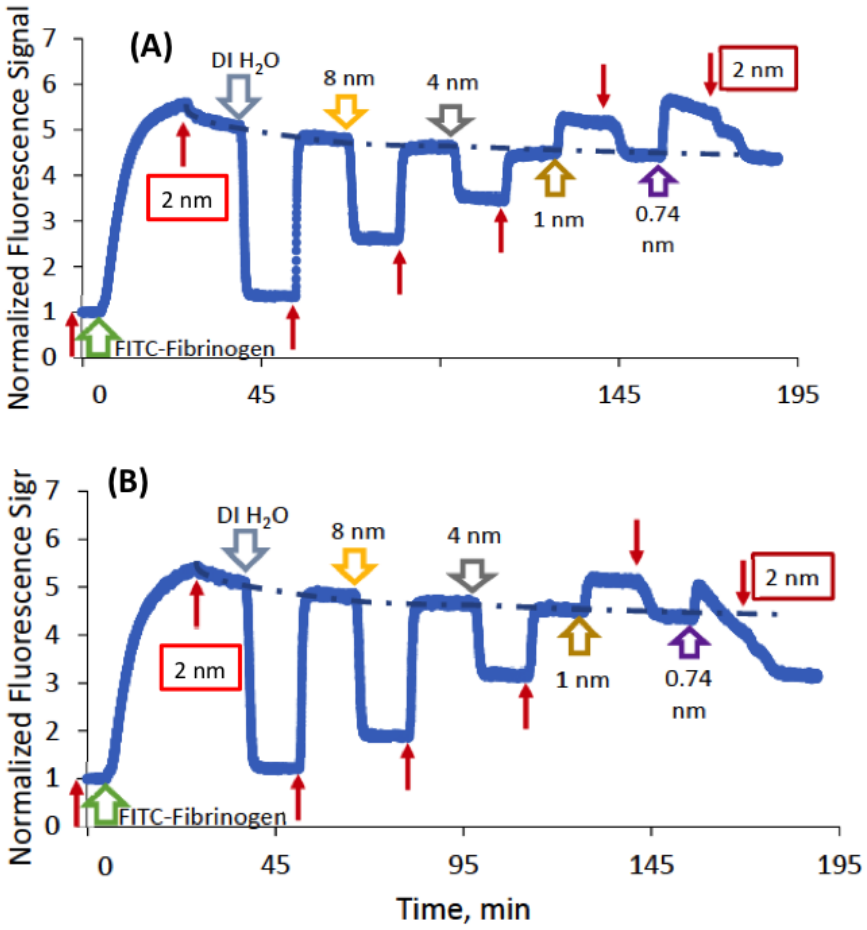

Figure 3. Examples of runs on (A) graphene and (B) silica showing FITC-fibrinogen adsorption followed by exposing the adsorbed layers to the different buffers, or DI water, indicated. The numbers, in nanometers on each run represent the Debye lengths of each buffer. The buffer having the Debye length of 2 nm, is the primary buffer of the study and is reinjected (the small red arrows beneath the data) repeatedly in between each test buffer.

The dominant feature of Figure 3 is the reversible change in fluorescence when the ionic strength of the buffer is changed at fixed pH 7.4. Most dramatically, the introduction of flowing DI water (which, in addition to the substantial reduction in ionic strength is accompanied by a pH decrease to near 6) produces a nearly complete fluorescence loss, which recovers fully when the original buffer is replaced. Ionic strengths lower than the

ACCEPTED MANUSCRIPT

0.026 M of the main buffer produce a fluorescence reduction while higher ionic strengths reversibly increase the fluorescence. An ionic strength of 1.026 M, producing a Debye length of κ^{-1} = 0.74 nm produces some loss of protein on the silica surface, ending the run.

The ionic strength effect on fluorescence is interfacial. Figure 4A summarizes the substantial impact of ionic strength of the fluorescence from FITC-fibrinogen adsorbed on supported graphene and on the bare silica. In order to compare the data, the fluorescence at each ionic strength was normalized on the that in κ^{-1} =2 nm buffer, using an average of the signal in the κ^{-1} =2 nm buffer just before and just after the injection of each test buffer, as in Figure 3. Then the data were renormalized again on the datum at κ^{-1} =1 nm, simply because this was the highest ionic strength that could be reliably measured without the complication of protein desorption. (This procedure for data renormalization eliminated run-run variations due to differences in label density among fibrinogen batches, the lamp intensity and detector voltage, etc. The result was highly reproducible normalized intensities in Figure 4A for multiple runs.) Evident in Figure 4A is a dramatic overall change in fluorescence along with modest differences between graphene and silica. The data represent averages for three surfaces of each type (with the error bars showing the range of data). The dashed line indicates the low fluorescence level in DI water.

Figure 4B provides, for comparison, the influence of ionic strength on the bulk solution fluorescence of FITC-fibrinogen, measured in a standard cuvette. The buffer solutions are the same as those employed with the graphene or silica surfaces. The fluorescence signal, also normalized for the buffer at κ^{-1} =1 nm is strong and independent of ionic strength in

ACCEPTED MANUSCRIPT

contrast to Figure 4A. The data in Figure 4B were measured at the relatively dilute FITC-fibrinogen concentration of 20 ppm, and also with unlabeled fibrinogen added to achieve the higher concentration of 12.5wt% fibrinogen. (We provide data for a high concentration because the interfacial environment is more concentrated in fibrinogen than the solutions from which fibrinogen adsorbs.) It is clear from Figure 4 that the ionic strength dependence of the fluorescence is a result of the interfacial environment and not a behavior seen in free fibrinogen solutions.

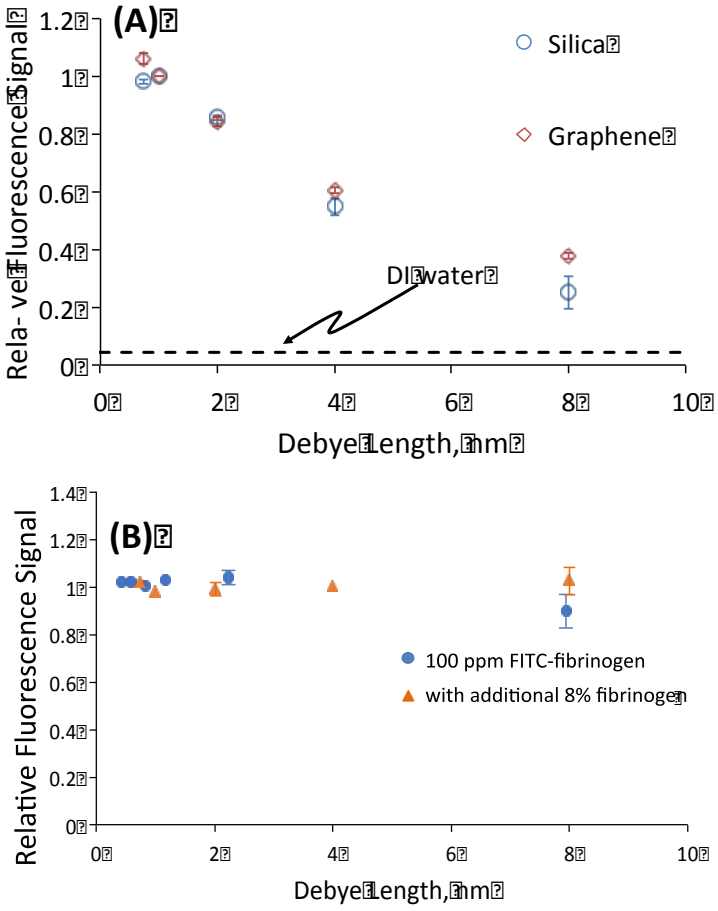

Figure 4. Impact of ionic strength (via Debye length) on fluorescence from FITC-fibrinogen. (A) With protein adsorbed on supported graphene or on silica, and (B) in free solution. Error bars represent range for 3-5 data points. USE THIS VERSION FOR REVIEW only. SEE high quality figure attached separately

ACCEPTED MANUSCRIPT

Quantitating the Near-Surface Environment

Fluorescein exists in solution in several forms, with the fluorescent dianion form persisting at neutral and higher pH. The monoanion is not fluorescent, and a pKa of 6.7 describes the equilibrium between the dianion and monoanion.[48, 49]

The aqueous environment near surfaces usually differs from the bulk solution, and the fluorescence from near- interface fluorescein reflects its local environment.[37, 50, 51] The near-surface acidity of silica, resulting from dissociation of surface silanols, is a well-studied example of an interfacial region that differs from the bulk solution. Depending on ionic strength, streaming potentials are measured in the range -30 to -90 mV.[52] The diffuse potential, ψ, beyond the first nanometer (approximately) from the surface, starting with ψ_s, is well-described by the Guoy Chapman treatment in its dependence on position x from the surface:

$$\boldsymbol{\Psi} = 2\, ln \frac{1+exp(-\kappa x)tanh(\boldsymbol{\Psi}_s/4)}{1-exp(-\kappa x)tanh(\boldsymbol{\Psi}_s/4)} \qquad (1)$$

Where $\boldsymbol{\Psi} = \frac{ez\psi}{kT}$, is a dimensionless potential, with e the charge on an electron, z the valence of the ions, and kT the thermal energy.

FITC labels on adsorbed fibrinogen in the neighborhood of the diffuse layer are expected to experience the local potential rather than the bulk pH.

ACCEPTED MANUSCRIPT

To estimate the effect of local potential on florescence from FITC labels on adsorbed fibrinogen, we combined the near-surface potential calculated from the Guoy Chapman equation with a Boltzmann distribution to model the local proton concentration. Then using the pKa for the fluorescein monoanion-dianion equilibrium, we calculated the fraction of near-surface FITC that would be in the fluorescent dianion form.

Figure 5 plots the predicted relative fluorescence (proportional to the fraction of FITC in dianion form and normalized on that for κ^{-1} =1 nm similar to the experiments of Figure 4) for the case where the FITC labels are positioned 2 nm from the start of the diffuse layer. Normalization on the value at an arbitrary Debye length eliminates the need to specify the local FITC concentration. Two different near-surface potentials at the start of the diffuse layer are considered to illustrate how the qualitative features of the ionic strength dependence are preserved independent of the actual values of ψ_s chosen. Since the exact position of FITC is unknown and likely encompasses a range, each of the two main curves are bracketed by a gray shaded area: The upper bound corresponds to a FITC position of 3 nm and the lower bound corresponds to a FITC position of 1nm. This exercise demonstrates that estimating the label placement too much further from the interface produces substantial discrepancy with observations.. Positioning the flouorophores 45 nm from the surface, the length of the fibrinogen adsorbed in an end-on conformation, would place labels outside the diffuse layer into the bulk solution where the ionic strength dependence is not expected. The observed large impact of ionic strength suggests that the

ACCEPTED MANUSCRIPT

fluorophores are indeed within a few nanometers of the start of the diffuse layer, a position that reflects interfacial charge.

Figure 5 agrees well with the experimental observations in Figure 4A. This suggests that the ionic strength dependence of the interfacial FITC-fibrinogen fluorescence results from changes in the near surface potential with ionic strength. An important implication of the qualitative similarities of graphene and silica is that the environment near silica- supported graphene is low-pH, though not quite so much as near bare silica.

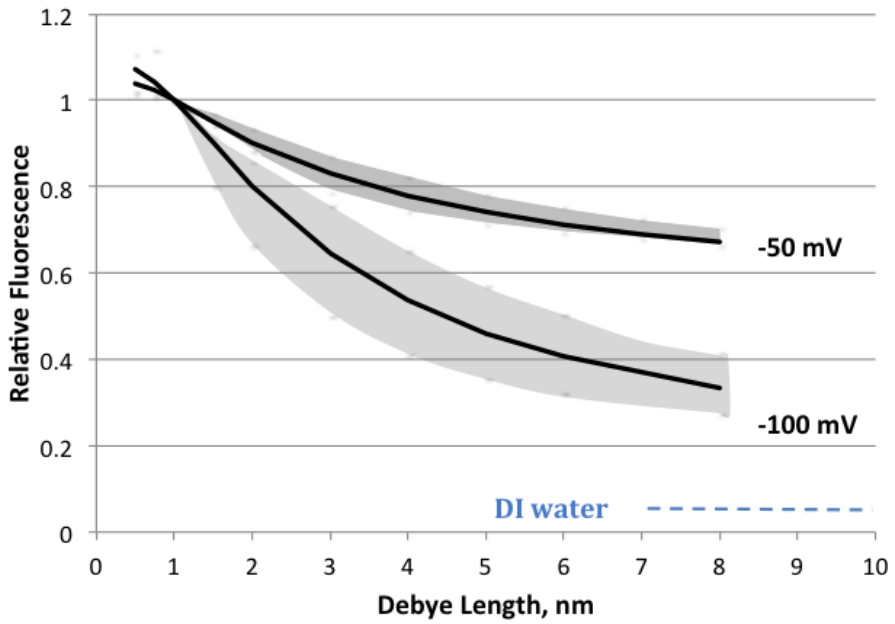

Figure 5. Calculated fluorescence from near-surface FITC, normalized on the value corresponding to a Debye length of 1 nm. Calculations are performed for the two potentials (shown) which start on the inside of the diffuse layer. The lines correspond to FITC positions of 2 nm. The gray areas bound the results for FITC positions of 1nm (lower bound) and 3 nm (upper bound).

ACCEPTED MANUSCRIPT

DISCUSSION

The signal from fluorescein tags on protein adsorbed to silica-supported graphene was found to be highly ionic-strength dependent and similar to that for protein adsorbed on silica in the absence of a graphene layer. This behavior could not be reproduced in free solution over the same range of buffer solutions, but was well-described by calculations of the proportion of near-surface fluorescein in the fluorescent dianion form. The calculation employed a range of estimates for the interfacial potential at the start of the diffuse layer and the fluorophore position. This range of inputs to the calculation was necessary because on silica and at the fibrinogen coverages observed, the long fibrinogen molecules assume a variety of interfacial orientations from end-on to side-on and in between,[40, 46, 47, 53] giving a range of fluorophore positions. Further, the aqueous environment near the fibrinogen may differ from bulk water or that within nm of bare silica/graphene, producing a different dielectric constant and the fibrinogen itself may produce a near –interfacial dielectric constant different from pure water. This would affect the calculations by altering the Debye length, a challenge common to quantifying the electrostatic environment in adsorbed layers in general. Thus the calculations represent a first approximation in the prediction of length scales for this system, but work quite well to demonstrate the mechanism of the salt-related fluorescence change. The ionic strength dependence arose in the calculations because as the Debye length was varied, the environment within a few nanometers of the surface switched from conditions similar to the bulk solution to those dominated by the interfacial acidity.

ACCEPTED MANUSCRIPT

With silica's negative surface charge well-established, (zeta potentials of -95, -60, and -25 mV for Debye lengths of 9.6, 3.0, and 0.96 nm at pH 7.4),[52] the ionic strength dependence of the fluorescence from near-surface fluorescein, bound to fibrinogen, is expected. Indeed, a similar effect was reported two decades ago for fluorescein-tagged polyethylene oxide adsorbed on silica.[51] Since PEO is a neutral polymer, very different from fibrinogen and its variety of chemical functionality, (hydrophobic, polar, and ionizable) one can argue that the fluorescein is more sensitive overall to the interfacial charge than to the charged groups on the fibrinogen. This possibility is consistent with Figure 4B: Attachment of fluorescein to fibrinogen does not produce an ionic strength dependence in free solution.

The parallel ionic strength dependencies, in Figure 4A, of fluorescence at the supported graphene and silica surfaces suggests a near-graphene environment dominated by negative charge, the range of which is controlled by ionic strength. This finding for supported graphene is unanticipated because of the lack of negatively-charged chemical functionality. Negative charge would typically arise from oxidized carbons, in the form of carboxylic acids and alcohols. Our supported graphene, however, showed no oxidation, which would also be accompanied by the presence of sp3 carbons, which were absent from the Raman spectra.[33] Our graphene surfaces were also mildly hydrophobic, with advancing contact angles of 76.8 °± 4.2°, arguing against charge originating from graphene itself.

Despite this argument against negative charge arising from the graphene chemistry, there is independent evidence of surface charge near silica-supported graphene. We recently observed that instead of adhering to silica-supported graphene as would be expected for a

ACCEPTED MANUSCRIPT

surface with little or no charge, micron-scale silica particles were non-adhesive towards supported graphene in pH 7 buffer at moderately low ionic strength.[33] However, silica particles did adhere to supported graphene at increased ionic strength at fixed pH of 7.[33] These observations ran qualitatively parallel to the ionic-strength dependence of silica sphere adhesion on silica itself, though, higher salt was needed to induce adhesion in the silica-silica system. The influence of salt on silica-sphere graphene adhesion suggested an adsorbed layer of negative ions in imparting negative charge near the graphene. Similar negative charge may be present on the graphene during protein adsorption however, one might expect that adsorbed protein would perturb a surface-layer of ions.

An alternate explanation is that, with silica-supported graphene, water can sufficiently access the space between the graphene and the silica support, enabling dissociation of silica's surface silanols. This dissociation sets up an acidic environment beneath the graphene, similar to the negative charge on bare silica. The ability of counterions to be influenced by the surface charge and to set up a diffuse layer near and beyond the graphene is not clear. However, to the extent that van der Waals forces from a surface can penetrate graphene to influence the water contact angle,[32] one would expect an electrostatic potential to also penetrate graphene: Both van der Waals and near-surface potential decays are electrostatic in nature.

The key observable difference, then the near-surface potentially at the start of the double layer: On silica, the calculations reveal a value near -85 to -90 mV to explain the observed extent of quenching while a slightly more modest value of ~ -75 mV would appear to be

ACCEPTED MANUSCRIPT

operate near the supported graphene. Both these estimates are more negative than those which were employed in calculations that matched the interactions of silica spheres with supported graphene or bare silica, (-50 mV, the same flat substrate systems.) The reason may be that the fluorophores may in fact be confined very close to the inner Helmholtz layer or the fibrinogen adsorption may perturb the near-surface potential distribution somewhat, allowing the labels to experience a more locally negative character than they would experience in simple buffer but confined near the surface in a thought experiment. Either way, however, the experiments, along with the modeling, show substantial parallels between silica supported graphene and silica itself, with a negative surface character arising from the underlying silica surface (with a field penetrating through the graphene) or the adsorption of anions to the graphene itself. The parallel behavior between independent fluorescence experiments and previously published colloidal interactions makes a strong case for this interpretation.

The current findings for negative interfacial charge near silica-supported graphene, and the possibility for electrostatic interactions from the underlying silica to pass through the graphene (consistent with our colloidal interaction study), is important because streaming potential studies on supported graphene are not yet possible. Even "large area graphene" such as that in the current work does not reliably produce specimens of sufficient size to measure streaming potential. Our typical graphene specimens were 5-7 mm on a side.

ACCEPTED MANUSCRIPT

Conclusions

The fluorescence from FITC-fibrinogen adsorbed onto silica-supported graphene in buffer exhibits a strong ionic-strength dependence, slightly weaker than that observed for FITC-fibrinogen adsorbed on silica. On supported graphene, the fluorescence in pH 7.4 buffer having a Debye length near 8 nm was 40% of that measured at the same pH and a Debye length near 1 nm. The fluorescence from the FITC-fibrinogen layer in DI water was less than 10% of that in pH 7.4 buffer and a Debye length of 10 nm. The fluorescence rapidly adjusts to changes in ionic strength of the buffer in the flow chamber.

These observations are consistent with calculations that take into account the pH-dependence of fluorescein and the elevated proton concentration near a negatively charged surface such as silica. In the case of graphene, the explanation also requires a near surface negative charge. Prior observations that silica spheres are repelled from silica-supported graphene at neutral pH and low ionic strength but become adhesive with increased ionic strength (as also occurs on bare silica) provide separate evidence of this negative interfacial character for supported graphene. Without charge on the graphene itself (evidence by the spectra in prior publications), the best explanation is that negative charge results from ion adsorption or from dissociation of surface silanols beneath the graphene.

The results emphasize the importance of controlling ionic strength when quantitatively interpreting fluorescence signals from near-graphene fluorescein labels. Further, because the dramatic influence of ionic strength occurs over the Debye length range 1-8 nm, this

ACCEPTED MANUSCRIPT

effect could be exploited as an interfacial ruler to tune fluorescence efficiency depending on the positions of fluorescein labels and the size of the target molecules.

Acknowledgements This work was supported by NSF 12-64855. ALB acknowledges the Office of Naval Research (N000141612612). We thank Yue Zhang and Hyunbok Lee for helpful discussions and synthesis of graphene.

ACCEPTED MANUSCRIPT

ACCEPTED MANUSCRIPT

REFERENCES

(1) de Miguel, M.; Alvaro, M.; Garcia, H. Graphene as a quencher of electronic excited states of photochemical probes. *Langmuir* **2012,** *28*, 2849-2857.
(2) Li, S. H.; Aphale, A. N.; Macwan, I. G.; Patra, P. K.; Gonzalez, W. G.; Miksovska, J.; Leblanc, R. M. Graphene oxide as a quencher for fluorescent assay of amino acids, peptides, and proteins. *ACS Appl. Mater. Interfaces* **2012,** *4*, 7068-7074.
(3) Park, J. S.; Goo, N. I.; Kim, D. E. Mechanism of DNA adsorption and desorption on graphene oxide. *Langmuir* **2014,** *30*, 12587-12595.
(4) Wang, Q. B.; Wang, W.; Lei, J. P.; Xu, N.; Gao, F. L.; Ju, H. X. Fluorescence quenching of carbon nitride nanosheet through its interaction with DNA for versatile fluorescence sensing. *Anal. Chem.* **2013,** *85*, 12182-12188.
(5) Ranganathan, S. V.; Halvorsen, K.; Myers, C. A.; Robertson, N. M.; Yigit, M. V.; Chen, A. A. Complex thermodynamic behavior of single-stranded nucleic acid adsorption to graphene surfaces. *Langmuir* **2016,** *32*, 6028-6034.
(6) Wang, Y.; Li, Z. H.; Wang, J.; Li, J. H.; Lin, Y. H. Graphene and graphene oxide: Biofunctionalization and applications in biotechnology. *Trends Biotechnol.* **2011,** *29*, 205-212.
(7) Dong, H. F.; Gao, W. C.; Yan, F.; Ji, H. X.; Ju, H. X. Fluorescence resonance energy transfer between quantum dots and graphene oxide for sensing biomolecules. *Anal. Chem.* **2010,** *82*, 5511-5517.
(8) He, S. J.; Song, B.; Li, D.; Zhu, C. F.; Qi, W. P.; Wen, Y. Q.; Wang, L. H.; Song, S. P.; Fang, H. P.; Fan, C. H. A graphene nanoprobe for rapid, sensitive, and multicolor fluorescent DNA analysis. *Adv. Funct. Mater.* **2010,** *20*, 453-459.
(9) Wen, Y. Q.; Xing, F. F.; He, S. J.; Song, S. P.; Wang, L. H.; Long, Y. T.; Li, D.; Fan, C. H. A graphene-based fluorescent nanoprobe for silver(i) ions detection by using graphene oxide and a silver-specific oligonucleotide. *Chem. Commun.* **2010,** *46*, 2596-2598.
(10) Feng, D.; Song, Y. C.; Shi, W.; Li, X. H.; Ma, H. M. Distinguishing folate-receptor-positive cells from folate-receptor-negative cells using a fluorescence off-on nanoprobe. *Anal. Chem.* **2013,** *85*, 6530-6535.
(11) Lee, J.; Park, I. S.; Park, G.; Cho, K.; Park, H. S.; Min, D. H. A robust and quantitative assay platform for multiplexed, high throughput screening of protein kinase inhibitors. *Chem. Commun.* **2016,** *52*, 12112-12115.
(12) Liu, Z. B.; Liu, B. W.; Ding, J. S.; Liu, J. W. Fluorescent sensors using DNA-functionalized graphene oxide. *Anal. Bioanal. Chem.* **2014,** *406*, 6885-6902.
(13) Kim, J.; Cote, L. J.; Kim, F.; Huang, J. X. Visualizing graphene based sheets by fluorescence quenching microscopy. *J. Am. Chem. Soc.* **2010,** *132*, 260-267.
(14) Lu, C.; Huang, P. J. J.; Liu, B. W.; Ying, Y. B.; Liu, J. W. Comparison of graphene oxide and reduced graphene oxide for DNA adsorption and sensing. *Langmuir* **2016,** *32*, 10776-10783.
(15) Song, E. Q.; Cheng, D.; Song, Y.; Jiang, M. D.; Yu, J. F.; Wang, Y. Y. A graphene oxide-based fret sensor for rapid and sensitive detection of matrix metalloproteinase 2 in human serum sample. *Biosens. Bioelectron.* **2013,** *47*, 445-450.
(16) Guzelturk, B.; Demir, H. V. Near-field energy transfer using nanoemitters for optoelectronics. *Adv. Funct. Mater.* **2016,** *26*, 8158-8177.

ACCEPTED MANUSCRIPT

(17) Tian, F.; Lyu, J.; Shi, J. Y.; Yang, M. Graphene and graphene-like two-denominational materials based fluorescence resonance energy transfer (fret) assays for biological applications. *Biosens. Bioelectron.* **2017,** *89*, 123-135.
(18) Yao, B. C.; Wu, Y.; Yu, C. B.; He, J. R.; Rao, Y. J.; Gong, Y.; Fu, F.; Chen, Y. F.; Li, Y. R. Partially reduced graphene oxide based fret on fiber-optic interferometer for biochemical detection. *Sci Rep* **2016,** *6*.
(19) Tan, A. T. L.; Kim, J.; Huang, J. K.; Li, L. J.; Huang, J. X. Seeing two-dimensional sheets on arbitrary substrates by fluorescence quenching microscopy. *Small* **2013,** *9*, 3253-3258.
(20) Bernardi, M.; Palummo, M.; Grossman, J. C. Extraordinary sunlight absorption and one nanometer thick photovoltaics using two-dimensional monolayer materials. *Nano Lett.* **2013,** *13*, 3664-3670.
(21) Ray, P. C.; Fan, Z.; Crouch, R. A.; Sinha, S. S.; Pramanik, A. Nanoscopic optical rulers beyond the fret distance limit: Fundamentals and applications. *Chem. Soc. Rev.* **2014,** *43*, 6370-6404.
(22) Treossi, E.; Melucci, M.; Liscio, A.; Gazzano, M.; Samori, P.; Palermo, V. High-contrast visualization of graphene oxide on dye-sensitized glass, quartz, and silicon by fluorescence quenching. *J. Am. Chem. Soc.* **2009,** *131*, 15576-+.
(23) Zhu, X. H.; Liu, Y.; Li, P.; Nie, Z.; Li, J. H. Applications of graphene and its derivatives in intracellular biosensing and bioimaging. *Analyst* **2016,** *141*, 4541-4553.
(24) Swathi, R. S.; Sebastian, K. L. Resonance energy transfer from a dye molecule to graphene. *J. Chem. Phys.* **2008,** *129*.
(25) Swathi, R. S.; Sebastian, K. L. Distance dependence of fluorescence resonance energy transfer. *J. Chem. Sci.* **2009,** *121*, 777-787.
(26) Swathi, R. S.; Sebastian, K. L. Long range resonance energy transfer from a dye molecule to graphene has (distance)(-4) dependence. *J. Chem. Phys.* **2009,** *130*.
(27) Garg, R.; Dutta, N. K.; Choudhury, N. R. Work function engineering of graphene. *Nanomaterials* **2014,** *4*, 267-300.
(28) Lee, H.; Puodziukynaite, E.; Zhang, Y.; Stephenson, J. C.; Richter, L. J.; Fischer, D. A.; DeLongchamp, D. M.; Emrick, T.; Briseno, A. L. Poly(sulfobetaine methacrylate)s as electrode modifiers for inverted organic electronics. *J. Am. Chem. Soc.* **2015,** *137*, 540-549.
(29) Zhang, L.; Ding, Z. C.; Tong, T.; Liu, J. Tuning the work functions of graphene quantum dot-modified electrodes for polymer solar cell applications. *Nanoscale* **2017,** *9*, 3524-3529.
(30) Kozbial, A.; Li, Z.; Conaway, C.; McGinley, R.; Dhingra, S.; Vahdat, V.; Zhou, F.; D'Urso, B.; Liu, H.; Li, L. Study on the surface energy of graphene by contact angle measurements. *Langmuir* **2014,** *30*, 8598-8606.
(31) Taherian, F.; Marcon, V.; van der Vegt, N. F. A.; Leroy, F. What is the contact angle of water on graphene? *Langmuir* **2013,** *29*, 1457-1465.
(32) Rafiee, J.; Mi, X.; Gullapalli, H.; Thomas, A. V.; Yavari, F.; Shi, Y. F.; Ajayan, P. M.; Koratkar, N. A. Wetting transparency of graphene. *Nature Materials* **2012,** *11*, 217-222.
(33) Chen, A. W.; Fang, B.; Lee, H.; Briseno, A. L.; Santore, M. M. Evidence for negative charge near large area supported graphene in water: A study of silica microsphere interactions. *J. Colloid Interface Sci.* **2017,** *492*, 15-24.
(34) Gao, L.; Li, Q.; Li, R. Q.; Yan, L. R.; Zhou, Y.; Chena, K. P.; Shi, H. X. Highly sensitive detection for proteins using graphene oxide-aptamer based sensors. *Nanoscale* **2015,** *7*, 10903-10907.

ACCEPTED MANUSCRIPT

(35) Wang, L.; Zhu, J. B.; Han, L.; Jin, L. H.; Zhu, C. Z.; Wang, E. K.; Dong, S. J. Graphene-based aptamer logic gates and their application to multiplex detection. *ACS Nano* **2012,** *6*, 6659-6666.
(36) Xing, X. J.; Liu, X. G.; He, Y.; Lin, Y.; Zhang, C. L.; Tang, H. W.; Pang, D. W. Amplified fluorescent sensing of DNA using graphene oxide and a conjugated cationic polymer. *Biomacromolecules* **2013,** *14*, 117-123.
(37) Wall, J.; Golding, C. A.; Vanveen, M.; Oshea, P. The use of fluoresceinphosphatidylethanolamine (fpe) as a real-time probe for peptide membrane interactions *Mol. Membr. Biol.* **1995,** *12*, 183-192.
(38) Robeson, J. L.; Tilton, R. D. Effect of concentration quenching on fluorescence recovery after photobleaching measurements *Biophysical Journal* **1995,** *68*, 2145-2155.
(39) Wertz, C. F.; Santore, M. M. Adsorption and relaxation kinetics of albumin and fibrinogen on hydrophobic surfaces: Single-species and competitive behavior. *Langmuir* **1999,** *15*, 8884-8894.
(40) Wertz, C. F.; Santore, M. M. Effect of surface hydrophobicity on adsorption and relaxation kinetics of albumin and fibrinogen: Single-species and competitive behavior. *Langmuir* **2001,** *17*, 3006-3016.
(41) Wasilewska, M.; Adamczyk, Z.; Jachimska, B. Structure of fibrinogen in electrolyte solutions derived from dynamic light scattering (dls) and viscosity measurements. *Langmuir* **2009,** *25*, 3698-3704.
(42) Wojciechowski, P. W.; Brash, J. L. Fibrinogen and albumin adsorption from human blood-plasma and from buffer onto chemically functionalized silica substrates. *Colloid Surf. B-Biointerfaces* **1993,** *1*, 107-117.
(43) Adamczyk, Z.; Bratek-Skicki, A.; Dabrowska, P.; Nattich-Rak, M. Mechanisms of fibrinogen adsorption on latex particles determined by zeta potential and afm measurements. *Langmuir* **2012,** *28*, 474-485.
(44) Fu, Z. G.; Santore, M. M. Poly(ethylene oxide) adsorption onto chemically etched silicates by brewster angle reflectivity. *Colloid Surf. A-Physicochem. Eng. Asp.* **1998,** *135*, 63-75.
(45) Toscano, A.; Santore, M. M. Fibrinogen adsorption on three silica-based surfaces: Conformation and kinetics. *Langmuir* **2006,** *22*, 2588-2597.
(46) Kubiak, K.; Adamczyk, Z.; Wasilewska, M. Mechanisms of fibrinogen adsorption at the silica substrate determined by qcm-d measurements. *J. Colloid Interface Sci.* **2015,** *457*, 378-387.
(47) Wasilewska, M.; Adamczyk, Z. Fibrinogen adsorption on mica studied by afm and in situ streaming potential measurements. *Langmuir* **2011,** *27*, 686-696.
(48) Smith, S. A.; Pretorius, W. A. Spectrophotometric determination of pka values for fluroescein using activity coefficient corrections. *Water S.A.* **2002,** *28*, 395-402.
(49) Lindquvist, L. A flash photolysis sutdy of fluroescein. *Ark. Kemi.* **1960,** *16*, 79-138.
(50) Lee, R. J.; Wang, S.; Low, P. S. Measurement of endosome ph following folate receptor-mediated endocytosis. *Biochim. Biophys. Acta-Mol. Cell Res.* **1996,** *1312*, 237-242.
(51) Rebar, V. A.; Santore, M. M. A total internal reflectance fluorescence nanoscale probe of interfacial potential and ion screening in polyethylene oxide layers adsorbed onto silica. *J. Colloid Interface Sci.* **1996,** *178*, 29-41.
(52) Scales, P. J.; Grieser, F.; Healy, T. W.; White, L. R.; Chan, D. Y. C. Electrokinetics of the silica solution interface - a flat-plate streaming potential study. *Langmuir* **1992,** *8*, 965-974.

ACCEPTED MANUSCRIPT

(53) Wertz, C. F.; Santore, M. M. Fibrinogen adsorption on hydrophilic and hydrophobic surfaces: Geometrical and energetic aspects of interfacial relaxations. *Langmuir* **2002,** *18*, 706-715.

ACCEPTED MANUSCRIPT

ACCEPTED MANUSCRIPT

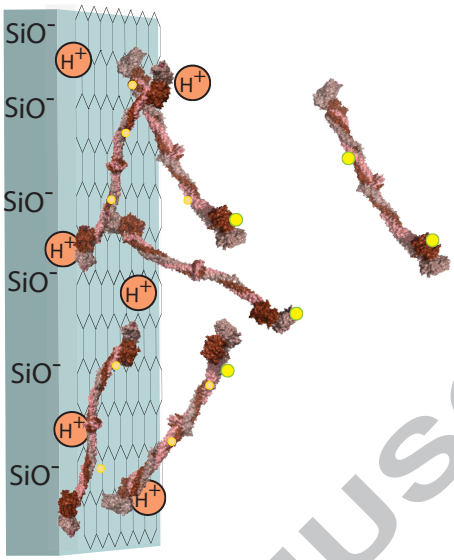

TOC Graphic

ACCEPTED MANUSCRIPT